Formation of a ZnS/Zn(S,O) bilayer buffer on CuInS$_2$ thin film solar cell absorbers by chemical bath deposition

M. Bär[a),b)]

Solarenergieforschung (SE2), Hahn-Meitner-Institut Berlin, Glienicker Strasse 100, D-14109 Berlin, Germany and Department of Chemistry, University of Nevada, 4505 Maryland Parkway, Las Vegas, Nevada 89145

A. Ennaoui,[a),c)] J. Klaer, T. Kropp, R. Sáez-Araoz, N. Allsop, I. Lauermann, H.-W. Schock, and M. C. Lux-Steiner[d)]

Solarenergieforschung (SE2, SE3), Hahn-Meitner-Institut Berlin, Glienicker Strasse 100, D-14109 Berlin, Germany

The application of Zn compounds as buffer layers was recently extended to wide-gap CuInS$_2$ (CIS) based thin film solar cells. Using an alternative chemical deposition route for the buffer preparation aiming at the deposition of a single-layer, nominal ZnS buffer without the need for any toxic reactants such as hydrazine has helped us to achieve a similar efficiency as respective CdS-buffered reference devices. In order to shed light on the differences of other Zn-compound buffers deposited in conventional chemical baths [chemical bath deposition (CBD)] compared to the buffer layers deposited by this alternative CBD process, the composition of the deposited buffers was investigated by x-ray excited Auger electron and x-ray photoelectron spectroscopy to potentially clarify their superiority in terms of device performance. We have found that in the early stages of this alternative CBD process a thin ZnS layer is formed on the CIS, whereas in the second half of the CBD the growth rate is greatly increased and Zn(S,O) with a ZnS/(ZnS+ZnO) ratio of ~80% is deposited. Thus, a ZnS/Zn(S,O) bilayer buffer is deposited on the CIS thin film solar cell absorbers by the alternative chemical deposition route used in this investigation. No major changes of these findings after a postannealing of the buffer/CIS sample series and recharacterization could be identified. © 2006 American Institute of Physics. [DOI: 10.1063/1.2202694]

I. INTRODUCTION

Achieving highly efficient Cd-free chalcopyrite thin film solar cells with efficiencies comparable to those obtained with the CdS buffer layer conventionally used in current state-of-the-art devices is an important milestone for the breakthrough of this thin film solar cell technology. At present, device (active area) efficiencies η up to 19.5% for low-gap ($E_g \leqslant 1.3$ eV) Cu(In,Ga)Se$_2$ (CIGSe) (Refs. 1 and 2) and around 12% for wide-gap CuInS$_2$ (CIS), (E_g^{CIS} = 1.54 eV) (Refs. 3–5) have been demonstrated. All these high efficiency values so far have been reported for solar cell devices with wet chemically deposited CdS buffer layers between the well-conducting n^+-ZnO/i-ZnO window bilayer and the chalcopyrite absorber. In most cases the CdS buffer is deposited in a chemical bath (CBD). However, CdS as a heavy metal compound should be avoided in the final solar modules as well as in their production processes from an ecological as well as an economical point of view. Furthermore, the low band gap of CdS (E_g = 2.4 eV) leads to a certain loss in the photocurrent by its absorption of the incoming solar radiation in the short-wavelength region.

Recently, various zinc compounds prepared by CBD have been attracting attention as alternative buffer materials and high efficiencies have already been demonstrated for corresponding low-gap chalcopyrite-based solar cells.[6–9] However, despite a higher transparency and thus a higher current collection in the blue wavelength region the direct comparison of the devices with Zn-compound buffer layers with the respective CBD-CdS buffered CIGSe-based solar cell reference shows an efficiency gap of ~1% (abs.).

In the past, Zn-compound buffer layers such as CBD-Zn(S,OH) developed for low-gap production scale Cu(In,Ga)(S,Se)$_2$ absorbers provided by Shell Solar GmbH (Munich, Germany) were also deposited at the Hahn-Meitner-Institut Berlin (HMI) (Berlin, Germany).[10–12] In this case, the obtained device efficiencies were comparable to those of corresponding CBD-CdS buffered references—independently confirmed by the National Renewable Energy Laboratory (NREL) (Golden, CO, U.S.A.).[12] Note that at this time the CBD process used still contained the highly toxic reactant hydrazine.[10–12]

However, when transferring this approach to wide-gap CIS-based solar cells, resulting devices with CBD-ZnS$_x$O$_y$H$_z$ buffers have yielded (active area) efficiencies of up to 10.7%,[13] whereas corresponding CBD-CdS buffered references reached 11.9%, showing again the efficiency gap of ~1% (abs.). Recent additional efforts initially aiming at a single-layer, nominal ZnS buffer CBD without the need of any toxic reactants such as hydrazine have helped us to close

a)Authors to whom correspondence should be addressed.
b)FAX: +1-702-895-4072; electronic mail: baerm2@unlv.nevada.edu
c)FAX: +49-(0)30-8062-3199; electronic mail: ennaoui@hmi.de
d)Also at Freie Universität Berlin, D-14195 Berlin, Germany.

the efficiency gap between corresponding Cd-free CIS solar cells with Zn-compound buffer layers and respective CdS-buffered reference devices. Resulting wide-gap CIS-based solar cells with a Zn-compound buffer deposited by this alternative chemical deposition route yielded comparable (total area) efficiencies (10.3%) to CdS-buffered references (10.4%).[14]

Since the parameters of the chemical bath deposition (*p*H value, temperature, complexing agents, deposition time, reactants and their concentration, application of ultrasound, rinsing solution, etc.) determine the properties of the prepared layer, there are as many different possible compositions (and consequently also notations) as CBD processes (see above). For a chemical bath consisting mainly of a Zn salt, thiourea, in some cases hydrazine,[10–13] and aqueous ammonia one can find in the literature notations for the composition of the deposited layers from as simple as CBD-ZnS (Ref. 6) over $Zn(S,OH)$,[10–12] $ZnS(O,OH)$,[7,9] $Zn(O,S,OH)_x$ (Ref. 8) to $ZnS_xO_yH_z$.[13] In consequence, the intention of this work is to determine the composition of our Zn-compound buffer layer, which results—as recently reported[14]—in a competitive device performance compared to corresponding CdS references when applied in wide-gap CIS-based solar cells. We aimed at finding possible differences in the composition compared to other Zn-compound buffer layers deposited by conventional CBD processes, shedding light on its superiority in terms of solar cell efficiency.

In order to investigate the growth mechanism of the alternative Zn-compound buffer layers on CIS/Mo/glass absorber substrates especially in terms of their (surface) composition, a complete set of samples (where the alternative buffer was deposited during different deposition times) was characterized by x-ray photoelectron spectroscopy (XPS) and x-ray excited Auger electron spectroscopy (XAES). In addition, ZnO, $Zn(OH)_2$, and ZnS reference layers also prepared on chalcopyrite/Mo/glass substrates were investigated for comparison.

II. EXPERIMENT

A. Preparation

1. CIS absorber

The CIS absorbers used in this study were prepared in the Technology Department of the HMI by sputter depositing the metallic In and Cu precursor layers on to Mo/glass substrates and subsequent sulfurization by rapid thermal processing using an excess of elemental sulfur vapor. More details on the preparation conditions are described in Ref. 3. The resulting CIS layers are Cu rich resulting in the formation of Cu_xS second phase precipitates on the absorber surface. However, these binary Cu compounds are removed very efficiently by KCN etching. Thus, before depositing the Zn-compound buffer layer, an additional etching step in a KCN-containing aqueous solution ($KCN_{aq}[3.5\%]$) was done to remove the segregated Cu_xS phases. After KCN etching the absorbers are then immediately stored in an aqueous solution containing ammonia ($NH_{3,aq}[2.5\%]$) prior to the buffer preparation.

2. Alternative Zn-compound buffer layer

For the preparation of the alternative Zn-compound buffer layer, we used an alternative CBD process, recently developed at the HMI Berlin,[15] aiming at the deposition of ZnS.

The entire amount of the Zn^{2+} precursor ($ZnSO_4 \cdot 7H_2O$; [0.15 mol/l]) is firstly mixed with thiourea ($SC(NH_2)_2$; [0.60 mol/l]) in an aqueous solution at 70–80 °C, leading to the formation of $[Zn(SC(NH_2)_2)_n]^{2+}$ complexes. Secondly, an excess of ammonia (NH_3) is then added to the bath solution under constant stirring, allowing the remaining Zn^{2+} ions (not bound in $[Zn(SC(NH_2)_2)_n]^{2+}$ complexes) to form $[Zn(NH_3)_n]^{+2}$ complexes with NH_3. The excess of ammonia is enough to keep the *p*H value of the chemical bath between 10 and 11, even during the CBD process. The *p*H of the solution was controlled using a 538WTW *p*H meter with temperature compensation and glass electrode (calibrated against standard *p*H 4 and 10 buffer solutions). Both thermal decomposition of the $[Zn(SC(NH_2)_2)_n]^{2+}$ and the reaction of $[Zn(NH_3)_n]^{+2}$ complexes with the released S^{2-} ions lead to the formation of ZnS. Usually after a certain time, which can vary from 10 to 20 min (depending on the bath conditions) a slightly milky solution is obtained. The substrates are then taken out of the chemical bath and washed in $NH_{3,aq}[2.5\%]$ solution in order to avoid an uncontrollable precipitation of $Zn(OH)_2$. This would take place if the sample (with residual Zn^{2+}-containing ammoniac solution on its surface) is rinsed in pure water. Then, the accompanied abrupt and drastic decrease of the *p*H value initiates the formation of $Zn(OH)_2$, which in consequence would precipitate on the sample. (A more detailed description of the deposition can be found in Refs. 14–17.)

In our case, the deposition was finished after 13.5 min. In this case, scanning electron micrographs of respective cross sections indicate a layer thickness of ~15 nm.[14] However, investigate the growth mechanism of the Zn-compound buffer especially in regard to layer composition for certain samples the CBD deposition was already interrupted after 3, 6, and 9 min. Hence, characterizing this set of buffer/CIS samples is considered to reveal a "time-resolved" (and thus "thickness-resolved") view on the layer composition prepared in the chemical bath.

After completion of the surface-spectroscopic characterization of the buffer/CIS samples, the entire series was annealed in system and thus in ultrahigh vacuum (UHV) at ~200 °C for 5 min. Subsequently, the complete sample series was recharacterized investigate the impact of the heat treatment on, e.g., their (surface) composition.

3. Zn(OH)₂, ZnO, and ZnS references

Additional samples were prepared for reference, as, e.g., a thin (~100 nm) ZnO layer deposited on a CIS absorber by rf magnetron sputtering was used as ZnO reference. Storing a similar sample in ambient air (for several days) opens the route for H_2O adsorption at the ZnO surface, which will lead to the formation of a surface $Zn(OH)_2$ layer as proposed in Refs. 18 and 19. This naturally generated hydroxide was used as $Zn(OH)_2$ reference. The ZnS reference in turn was

prepared by the spray-ILGAR (ion layer gas reaction) technique,[20] which provides samples with nearly stoichiometric composition as proven by elastic recoil detection analysis.[21] Note that in some cases the reference samples were Ar$^+$ etched (energy=3 keV and sample current ~1 μA) remove surface contaminants.

B. Characterization

In order to evaluate the surface composition of the buffer layers of various thicknesses, we characterized the entire buffer/CIS sample series by XAES and XPS measurements, which were performed using a Mg $K\alpha$ x-ray source (1253.56 eV). To minimize contamination from ambient air, the samples to be characterized were sealed in a polyethylene bag filled with N$_2$ immediately after preparation (which was done in air). Then, the samples were transferred into the analysis chamber of a combined ultrahigh vacuum preparation and spectroscopy system ("CISSY," see Ref. 22 for more details) at a base pressure of $<1 \times 10^{-9}$ mbar via an attached N$_2$ filled glove box. A CLAM4 electron spectrometer from Thermo VG Scientific was used for electron detection. The electron spectrometer was calibrated according to Ref. 23 using XPS and Auger line positions of different metals (Cu $3p$, Au $4f_{7/2}$, Cu L_3MM, and Cu $2p_{3/2}$).

For quantitative analysis, we fitted the photoemission signals by Voigt functions. Note that our fit procedure also included a linear background. In order to estimate the thickness of the buffer layer, we used the attenuation of the CIS substrate signals by the increasingly thick buffer applying Eq. (1),

$$I = I_0 \cdot e^{-d/\lambda}, \tag{1}$$

where I is the intensity of the respective (attenuated) photoemission signal, I_0 is the unattenuated signal intensity of the bare (KCN-etched) CIS substrate, λ is the inelastic mean free path of the corresponding photoelectrons, and d is the thickness of the attenuating buffer layer. λ was calculated by the TPP-2 formula[24] using the QUASES code written by Tougaard,[25] which provides values with an assumed absolute uncertainty of ~20%.

III. RESULTS AND DISCUSSION

Figure 1 shows the XPS survey spectra of the buffer/CIS sample series, where the nominal ZnS layer was deposited during different deposition times: (b) 3, (c) 6, (d) 9, and (e) 13.5 min). In addition, the respective spectrum (a) of a corresponding, uncovered (KCN-etched) CIS substrate is also presented. For the bare CuInS$_2$ sample all detected photoelectron and Auger electron signals can be ascribed to absorber's components as well as to (adventitious) carbon and oxygen. The latter is probably a remainder (adsorbed water) from the wet-chemical removal of the Cu$_x$S surface phase by KCN etching. For the spectra of the buffer/CIS series, an intensity decrease of all CIS attributed XPS and XAES signals can be observed with an increasing deposition time. (One exception are the peaks which correspond to sulfur, because also the nominal ZnS cover layer contains S.) Best visible is this attenuation effect for the prominent Cu $2p$ and
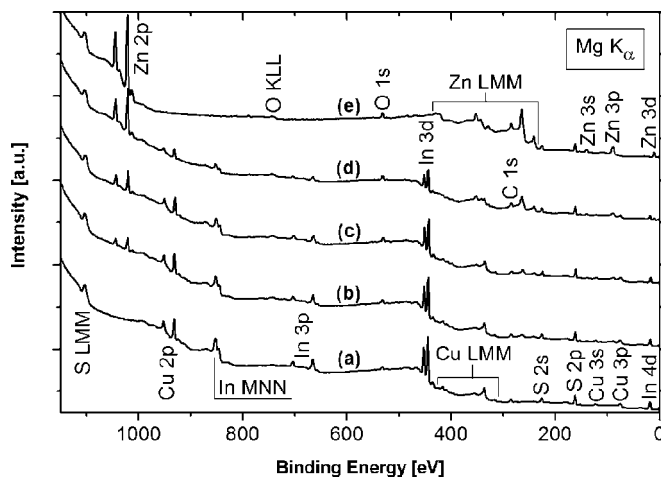

FIG. 1. XPS survey spectra of the buffer/CIS sample series, where the nominal ZnS buffer layers were deposited by different deposition times: (b) 3, (c) 6, (d) 9, and (e) 13.5 min. In addition, the respective spectrum (a) of a corresponding, uncovered (KCN-etched) CIS substrate is also presented.

In $3d$ XPS signals at ~940 and 450 eV binding energies E_B, respectively. At the same time, i.e., with an increasing deposition time, an increase of the Zn-related photoelectron and Auger electron signals can be noticed. (Note that distinct Zn-related XPS and XAES peaks can clearly be detected after already 3 min deposition time.) Close inspection of the data shows that also the XPS and XAES signals attributed to oxygen undergo a similar but by far less pronounced intensity increase as the Zn-related peaks (especially for the "9" and "13.5 min" samples), pointing to a certain oxide content in those buffer layers. However, as the Zn-compound layer is deposited wet chemically, the oxygen signals might not be a suitable measure for the composition of the alternative buffer as they could also stem from aqueous adsorbates. For the buffer/CIS sample, where the nominal ZnS layer was deposited within 13.5 min, no Cu- or In-attributed signals can be observed anymore. Thus, the 13.5 min buffer layer covers the rough CIS substrate completely with a minimal thickness which exceeds the XPS information depth. The latter is considered to be three times the inelastic mean free path λ of the respective photoelectrons[23] (accounting for an attenuation of 95% of the initial intensity) and thus is energy dependent. Assuming that, e.g., the In $3d_{5/2}$ ($E_B \approx 444$ eV) photoelectrons were exclusively attenuated by a pure ZnS layer, which covers the CIS absorber homogeneously, one can estimate the thickness of this cover layer to be $\geq (5.4 \pm 1.1)$ nm (based on the λ taken from Ref. 25).

In order to investigate the actual surface composition of the nominal ZnS layers on CIS the Zn $L_3M_{45}M_{45}$ XAES spectrum was evaluated, since this signal is more sensitive with respect to chemical shifts compared to most Zn photoemission lines (see below). Figure 2 (bottom) shows the XAES detail spectra of the ZnS/CIS sample series. The intensity of the Zn $L_3M_{45}M_{45}$ XAES signal increases with deposition time due to the increasingly thick buffer layer. This effect is more pronounced especially for the samples where the deposition was stopped in the second half of the CBD (deposition time ≥ 9 min). This is also supported by the increase of the Zn-related photoemission signals as well
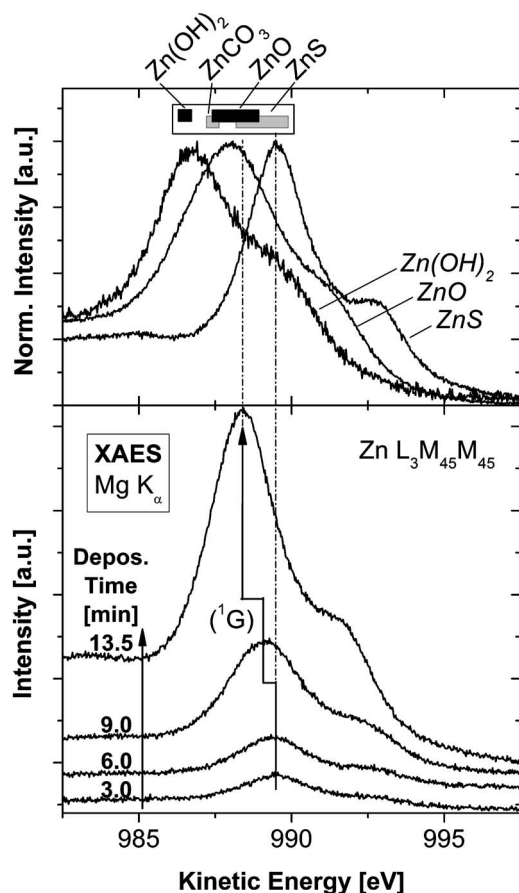
FIG. 2. Bottom: XAES detail spectra of the Zn $L_3M_{45}M_{45}$ Auger peak as measured on the samples of the buffer/CIS series. Top: Reference spectra of some Zn compounds deposited on chalcopyrite absorbers, such as Zn(OH)$_2$, ZnO, and ZnS, are also presented for comparison. The energetic positions of the Zn $L_3M_{45}M_{45}$ (^1G) Auger signal for different Zn compounds are additionally given as bars, representing their range of variation found in Refs. 26 and 27. (Note that in cases where only a single literature value is reported an error of ±0.2 eV, as suggested in Ref. 28, was assumed to represent its uncertainty.)

TABLE I. Energetic positions of the Zn $L_3M_{45}M_{45}$ (^1G) Auger peak as found for the buffer/CIS sample series and some Zn-compound references as Zn (OH)$_2$, ZnCO$_3$ ZnO, and ZnS compared to corresponding literature data. (Ref. 26 and 27. All experimentally determined values have an error of ±0.1 eV. In cases where only a single literature value is reported an error of ±0.2 eV as suggested in Ref. 28 was assumed to represent its uncertainty.

	Expt. Zn $L_3M_{45}M_{45}$ (^1G) E_{kin} (eV)	Literature Zn $L_3M_{45}M_{45}$ (^1G) E_{kin} (eV)
Buffer/CIS		
3 min	989.5	/
6 min	989.5	/
9 min	989.2	/
13.5 min	988.4	/
References		
Zn(OH)$_2$	986.7	986.2±0.2
ZnCO$_3$	/	987.4±0.2
ZnO	988.0	987.4−988.9
ZnS	989.5	988.2−989.9

cal bath [e.g., ZnO, ZnS, Zn(OH)$_2$, and ZnCO$_3$] provides many different values for the same material (see Table I). For ZnS, for example, one finds the Zn $L_3M_{45}M_{45}$ (^1G) signal at $E_{kin}=988.2−989.9$ eV.[26,27] Thus, the reference positions of the Zn $L_3M_{45}M_{45}$ (^1G) peak for the different Zn compounds are given as bars in Fig. 2 (top), representing the range of variation found in Refs. 26 and 27. (Note that in cases where only a single literature value is reported an error of ±0.2 eV as suggested in Ref. 28 is assumed to represent its uncertainty.) Moreover, in order to assure a better comparability, measured spectra of some Zn-compound references deposited on chalcopyrite absorbers, such as Zn(OH)$_2$ ZnO, and ZnS, are also presented in Fig. 2 (top). The energetic positions of their Zn $L_3M_{45}M_{45}$ (^1G) peaks [$E_{kin}^{Zn(OH)2}=(986.7±0.1)$ eV, $E_{kin}^{ZnO}=(988.0±0.1)$ eV, and $E_{kin}^{ZnS}=(989.5±0.1)$ eV] agree very well with the literature data (see Table I).

The comparison of the position of the Zn $L_3M_{45}M_{45}$ (^1G) Auger line of the measured XAES spectra of the nominal ZnS/CIS sample series (989.5−988.4) eV with the measured reference spectra as well as with the literature data suggests that for the thickest buffer layer (13.5 min) a Zn(S,O)-like surface composition with only minor amounts of ZnCO$_3$ or Zn(OH)$_2$ is most probable since the energetic position of its Zn $L_3M_{45}M_{45}$ (^1G) Auger peak (988.4±0.1) eV can be found between that of ZnO [experiment: (988.0±0.1) eV; literature: 987.4−988.9 eV] and ZnS [experiment: (989.5±0.1) eV; literature: 988.2−989.9 eV]. The hydroxide-poor composition is in contrast to several other publications reporting on Zn compounds deposited by CBD,[7–13] but can be explained by the rinsing step in an aqueous ammonia-containing solution after the material deposition in the chemical bath, avoiding an uncontrolled Zn(OH)$_2$ precipitation on the sample.[29] The Zn $L_3M_{45}M_{45}$ (^1G) Auger peak of the nominal ZnS/CIS samples prepared by shorter deposition times shifts to higher kinetic energies with decreasing deposition times until it actually agrees (for the "3" and "6 min" samples) quite well with the energetic position

as by the attenuation of the absorber peaks. Both show a corresponding behavior; a more pronounced increase or a more pronounced attenuation, respectively, for those samples (see survey spectra in Fig. 1). The growth rate in the early stages of the deposition (deposition time ≤6 min) is apparently much smaller compared to that of the consecutive time in the chemical bath, which points to a deposition-time dependent growth mechanism of the alternative buffer layer.

Moreover, one can observe that the Zn $L_3M_{45}M_{45}$ (^1G) Auger peak shifts from a kinetic energy E_{kin} of (989.5±0.1) eV for a deposition time of 3 min to (988.4±0.1) eV for the 13.5 min buffer/CIS sample. Note that this energetic shift is not caused by an interface formation induced band bending (see discussion of the corresponding Auger parameters below). Together with the behavior of the O-related XPS and XAES signals (see Fig. 1), which increase especially for the 9 and 13.5 min samples this points to a deposition time and thus thickness dependent change in composition in the nominal ZnS buffer layer. A literature enquiry[26,27] for reference positions for the Zn $L_3M_{45}M_{45}$ (^1G) Auger peak of Zn compounds possibly formed in the chemi-
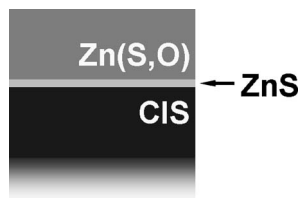
FIG. 3. Schematic illustration of the situation at the buffer/CIS interface as found after the applied alternative chemical deposition route for the preparation of a nominal ZnS layer, showing the resulting ZnS/Zn(S,O) bilayer buffer on top of the CIS substrate.

of the Zn $L_3M_{45}M_{45}$ (^1G) Auger peak of the ZnS reference as well as with the literature data for ZnS (see Fig. 2 and Table I). From this, one can conclude that the material deposition in the chemical bath of the alternative chemical route takes place in two steps. In the early stages of the deposition (3 and 6 min samples) primarily a thin ZnS layer is formed on the CIS substrate. Then, in the second half of the deposition (9 and 13.5 min samples) the growth rate is greatly increased compared to that of the initial stages of the CBD (see above) and a Zn(S,O) compound is deposited. A summary of these findings is represented in a schematic illustration (Fig. 3) showing a ZnS/Zn(S,O) bilayer buffer on top of the CIS substrate.

Whether the formation of the ZnS layer in the early stages of the CBD takes place between the S^{2-} ions released from the thiourea and the Zn^{2+} ions present in the chemical bath or whether at this point there are not yet S^{2-} ions released in the solution and the S-containing absorber surface acts as source for the anion has still to be clarified. The latter mechanism would be quite similar to the formation of a thin CdS or CdSe layer on S- or Se-containing chalcopyrite absorber (as reported elsewhere[30–32]) by means of a treatment in a so called "partial electrolyte"[33] exclusively containing the respective cations and aqueous ammonia but no chemically active anion source. In order to clarify this issue the next consequential step would be the XPS and XAES characterizations of a CIS sample treated in a solution quite similar to the chemical bath used in this investigation but without any S source. Unfortunately, the CBD process applied uses thiourea as complexing agent for the Zn^{2+} ions and thus cannot be easily omitted or replaced without a distinct impact on the entire deposition mechanism. Alternatively, in the future one could use a S-free substrate in order to check whether also in this case a ZnS/Zn(S,O) bilayer is formed. However, assuming that the ZnS is formed under participation of the CIS surface, this mechanism is likely to take place in most CBD processes (based on aqueous ammonia) and would not be restricted to the chemical deposition route used here.

With regard to the determination of the ZnS/(ZnS +ZnO) ratio of the deposited buffer layers one has to keep in mind that the samples were wet chemically prepared in a chemical bath and thus their surface may be contaminated by O- and C-containing compounds. In consequence, using the quantitatively evaluated O-related photoemission signal intensities for the calculation of the ZnS/(ZnS+ZnO) ratio might lead to falsified values. Thus, we have chosen an alternative approach to determine the buffer composition.
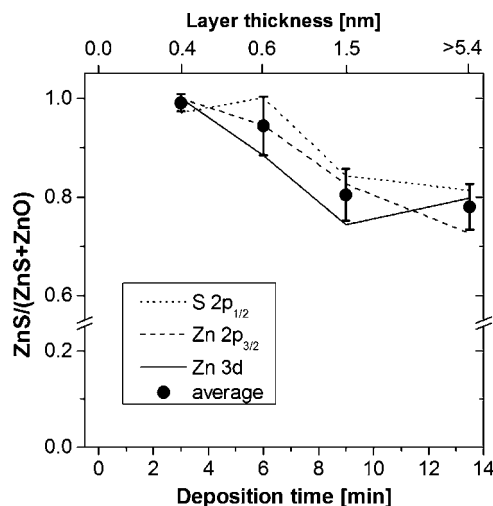

FIG. 4. ZnS/(ZnS+ZnO) compositions of the deposited buffer layers as function of their deposition time, determined from the intensity change of the S $2p_{1/2}$ XPS signal (dotted line) as well as from the ratio of the different contributions [I] (→ZnS) and [II] (→ZnO) to the Zn $2p_{3/2}$ (dashed line) and the Zn $3d$ photoemission lines (solid line). The corresponding averaged composition is also shown (bullets). The given error represents the standard deviation of each independently determined ZnS/(ZnS+ZnO) value from the corresponding mean composition. On top a scale is given, which relates the deposition time to the calculated thickness of the buffer layers.

Impurity-free and stochiometric ZnS contains 50% S. Assuming that the investigated Zn(S,O) layers are also impurity-free and hence are exclusively composed of the cation Zn^{2+} and either the anion S^{2-} or O^{2-}, then one would expect an intensity decrease in the S-related photoemission lines if the composition changes from pure ZnS to Zn(S,O). Assuming that for all samples the signal attenuation due to surface contamination is similar, any change in the XPS peak intensities ascribed to S (in our case S $2p_{1/2}$) can then be translated into a change of the ZnS/(ZnS+ZnO) ratio. Since $CuInS_2$ contains relatively the same amount of S as ZnS, the substrate will not interfere in this matter. Moreover, in a first approximation it can be used as reference for the S $2p_{1/2}$ signal intensity for a pure sulfide layer. The, respectively, normalized intensities of the S $2p_{1/2}$ photoemission line of the samples of the buffer/CIS series, which correspondingly represent the ZnS/(ZnS+ZnO) ratio of the deposited layers, are shown in Fig. 4 (dotted line).

In order to cross-check our approach to use the intensity change of the S $2p_{1/2}$ XPS signals to determine the ZnS/(ZnS+ZnO) ratio in the deposited buffer layers, we investigated also Zn-related photoemission lines. Despite the fact that these signals are not as sensitive to chemical changes as the corresponding Zn $L_3M_{45}M_{45}$ Auger spectra (Fig. 2), one can, however, identify shifts of 0.7 and 0.8 eV in the Zn $2p_{3/2}$ and Zn $3d$ photoemission signals, respectively, of the ZnO [$E_B^{Zn\,2p3/2}=(1022.4\pm0.1)$ eV; $E_B^{Zn\,3d}=(10.9\pm0.1)$ eV] and ZnS [$E_B^{Zn\,2p3/2}=(1021.7 \pm0.1)$ eV; $E_B^{Zn\,3d}=(10.1\pm0.1)$ eV] references, as shown in the top of Figs. 5 and the bottom of Tables II and III. Since the majority of the literature data regarding the energetic position of the Zn $3d$ XPS signal can be found for the entire Zn $3d$ and not for, e.g., the Zn $3d_{3/2}$ or the Zn $3d_{5/2}$ peak, the energetic position of the centroid of the respective fit of the
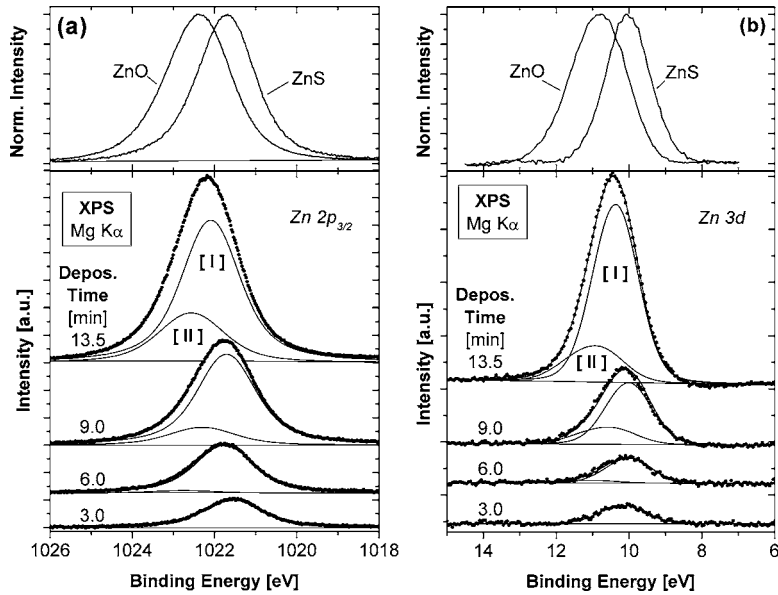
FIG. 5. Bottom: XPS detail spectra of the Zn $2p_{3/2}$ (a) and Zn $3d$ (b) photoemission signals of the buffer/CIS samples (bullets). The fit curves for contributions [I] ($\rightarrow$ZnS) and [II] ($\rightarrow$ZnO) to the corresponding XPS peaks are also presented (solid lines). [Note that for the presentation of the respective Zn $3d$ photoemission lines a proper fraction of a respective spectrum of an uncovered (KCN-etched) CIS sample was subtracted from the spectra of the buffer/CIS sample series in order to eliminate the influence of the background.] Top: XPS detail spectra of the Zn $2p_{3/2}$ (a) and Zn $3d$ (b) photoemission signals of ZnO and ZnS reference samples are shown for comparison.

Zn $3d$ photoemission line is given. However, in our data evaluation we appreciated the Zn $3d_{3/2}$. Zn $3d_{5/2}$ splitting by fitting the Zn $3d$ peak with two related Voigt functions. The doublet separation was found to be (0.83 ± 0.10) and (0.55 ± 0.10) eV for ZnO and ZnS, respectively. Taking the error bar into account, the experimentally determined values are in good agreement with the values discovered for metallic Zn [$(0.54-0.76)$ eV (Ref. 27)], which are the only respective data found in the literature. The experimentally determined energetic positions of the Zn $2p_{3/2}$ and Zn $3d$ XPS signals of the ZnO and ZnS references, respectively, agree also quite well with the respective literature data [$E_B^{\text{Zn }2p3/2}(\text{ZnO}_{\text{literature}})=(1021.2-1022.5)$ eV, $E_B^{\text{Zn }3d}(\text{ZnO}_{\text{literature}})=(10.3-10.8)$ eV $E_B^{\text{Zn }2p3/2}(\text{ZnS}_{\text{literature}})=(1021.7-1022.0)$ eV $E_B^{\text{Zn }3d}(\text{ZnS}_{\text{literature}})=(9.8-10.7)$ eV; see Tables II and III]. The Zn $2p_{3/2}$ and the Zn $3d$ photoemission lines of the samples of the buffer/CIS series are also shown in Figs. 5. [Note that for the Zn $3d$ XPS signals a

proper fraction of a respective spectrum of an uncovered (KCN-etched) CIS sample was subtracted from the spectra of the buffer/CIS samples in order to eliminate the influence of the background.] Similar to the behavior of the Zn $L_3M_{45}M_{45}$ Auger signal also the photoemission peaks shift with an increasing deposition time from a binding energy, which roughly correlates with the energetic position of the respective peaks for the ZnS reference (for the buffer/CIS samples where the deposition was stopped in the early stages of the CBD), to higher binding energies towards the energetic position of the Zn $p_{3/2}$ and Zn $3d$ XPS signals of the ZnO reference (for thicker buffer layers). This supports the conclusion from above that the deposition of the alternative buffer layer on to CIS substrates by the CBD process used in this investigation results in the formation of a ZnS/Zn(S,O) bilayer. Thus, the Zn $2p_{3/2}$ and Zn $3d$ spectra of the buffer/CIS samples are partially composed of a ZnS [I] and a ZnO [II] contribution. In consequence, the Zn $2p_{3/2}$ and Zn $3d$ XPS

TABLE II. Energetic positions of the two contributions ([I]$\rightarrow$ZnS and [II]$\rightarrow$ZnO) to the Zn $2p_{3/2}$ photoemission line as found for the buffer/CIS sample series. In addition, the corresponding values for the modified Auger parameter $\alpha'_1=E_{\text{kin}}$ [Zn $L_3M_{45}M_{45}(^1G)$]$+E_B$ [Zn $2p_{3/2}$] calculated using the values from Table I are also presented. For comparison the energetic positions of the Zn $2p_{3/2}$ XPS signal and the respective values for α'_1 of a ZnO and a ZnS reference as well as corresponding literature data (Ref. 26 and 27) are also given. All experimentally determined values have an error of ±0.1 eV.

Contribution	Expt. Zn $2p_{3/2}$ E_B (eV) [I]	[II]	Literature Zn $2p_{3/2}$ E_B (eV)	Expt. α'_1 (eV) [I]	[II]	Literature α'_1 (eV)
Buffer/CIS						
3 min	1021.6	/	/	2011.1	/	/
6 min	1021.8	1022.8	/	2011.3	2012.3	/
9 min	1021.7	1022.3	/	2010.9	2011.5	/
13.5 min	1022.1	1022.6	/	2010.5	2011.0	/
References						
ZnO		1022.4	1021.2–1022.5		2010.4	2009.5–2011.0
ZnS	1021.7		1021.7–1022.0	2011.2		2010.3–2011.9

TABLE III. Energetic positions of the two contributions ([I]→ZnS and [II]→ZnO) to the Zn 3d photoemission line as found for the buffer/CIS sample series. In addition, the corresponding values for the modified Auger parameter $\alpha'_2 = E_{kin}$ [Zn $L_3M_{45}M_{45}$(^1G)]$+E_B$ [Zn 3d] calculated using the values from Table I are also presented. For comparison the energetic positions of the Zn 3d XPS signal and the respective values for α'_2 of a ZnO and a ZnS reference as well as corresponding literature data (Ref. 26 and 27) are also given. All experimentally determined values have an error of ±0.1 eV. Note that no reference values for α'_2 were found in the literature.

Contribution	Expt. Zn 3d E_B (eV) [I]	[II]	Literature Zn3d E_B (eV)	Expt. α'_2 (eV) [I]	[II]
Buffer/CIS					
Zn(S,O); 3 min	10.2	/	/	999.7	
Zn(S,O); 6 min	10.0	11.1	/	999.5	1000.6
Zn(S,O); 9 min	310.0	10.6	/	999.2	999.8
Zn(S,O); 13.5 min	10.4	11.0	/	998.8	999.4
References					
ZnO		10.9	10.3–10.8		998.9
ZnS	10.1		9.8–10.7	999.6	

spectra of the buffer/CIS samples were fitted with two Voigt functions or with two doublets of related Voigt functions, respectively. Note that the determined full width at half maximum (FWHM) values of the photoemission signals of the ZnS (FWHM$^{Zn\,2p3/2}$=1.69 eV and FWHM$^{Zn\,3d}$=1.47 eV) and ZnO references (FWHM$^{Zn\,2p3/2}$=1.90 eV and FWHM$^{Zn\,3d}$=1.85 eV) and for the Zn 3d signals also their doublet separation were used and kept constant during the respective fit of the Zn $2p_{3/2}$ and Zn 3d spectra of the buffer/CIS samples. The resulting fits are shown in Fig. 5. Note that for the 3 min buffer/CIS sample satisfactory fits of the respective Zn-related photoemission lines were only achieved when only contribution [I] was assumed. This supports the conclusion from above that only a single Zn compound (ZnS) is formed on the CIS substrate in this case. Taking the error bars into account the determined energetic positions of contributions [I] and [II] to the respective Zn-related photoemission signals ($E_B^{Zn\,2p3/2}$[I]=(1021.6−1022.1) eV, $E_B^{Zn\,2p3/2}$[II]=(1022.3−1022.8) eV and $E_B^{Zn\,3d}$[I]=(10.0−10.4) eV, $E_B^{Zn\,3d}$[II]=(10.6−11.1) eV) agree quite well with the energetic positions of the ZnO and ZnS references as well as with corresponding literature data (see Tables II and III).

In order to exclude any impact of a varying band bending [potentially associated with a thicker growing (*n*-type) buffer layer deposited on a (*p*-type) CIS absorber] on the analysis of the energetic positions of the XAES and XPS signals and thus on the connected evaluation of the buffer composition we consider in the following also the modified Auger parameter. The values of the modified Auger parameters $\alpha'_1 = E_{kin}$ [Zn $L_3M_{45}M_{45}$(^1G)]$+E_B$[Zn $2p_{3/2}$] and $\alpha'_2 = E_{kin}$ [Zn $L_3M_{45}M_{45}$(^1G)]$+E_B$[Zn 3d] calculated for the contributions [I] and [II] to the Zn-related photoemission signals of the buffer/CIS samples decrease with deposition time (α'_1[I]=(2011.1±0.1) eV for 3 min to (2010.5±0.1) eV for 13.5 min, α'_1[II]=(2012.3±0.1) eV for 6 min to (2011.0±0.1) eV for 13.5 min and α'_2[I]

=(999.7±0.1) eV for 3 min to (998.8±0.1) eV for 13.5 min, α'_2[II]=(1000.6±0.1) eV for 6 min to (999.4±0.1) eV for 13.5 min). The values of contribution [I] agree quite well with the corresponding Auger parameters of ZnS [experiment: α'_1=(2011.2±0.1) eV, α'_2=(999.6±0.1) eV and literature: α'_1=(2010.3±2011.9) eV] for samples, where the deposition was stopped in the early stages of the deposition. In contrast, the determined Auger parameters of contribution [II] converge towards α'_1 as well as α'_2 of ZnO [experiment: α'_1=(2010.4±0.1) eV, α'_2=(998.9±0.1) eV and literature: α'_1=(2009.5±2011.0) eV] with an increasing deposition time (see Tables II and III). Note that for α'_2 no reference data could be found in the literature. All these findings support again the conclusion from above that the buffer deposition on to CIS substrates forms a ZnS/Zn(S,O) bilayer by using the CBD process applied in this investigation.

Using the areas below the fit curves, which describe contributions [I] (→ZnS) and [II] (→ZnO) to the Zn $2p_{3/2}$ and Zn 3d XPS spectra of the buffer/CIS sample series in Figs. 5, the ZnS/(ZnS+ZnO) ratios were calculated. The values determined from the Zn $2p_{3/2}$ and the Zn 3d photoemission lines are shown as function of the deposition time as dashed and solid lines, respectively, in Fig. 4. Both show a quite comparable behavior and additionally resemble quite well the ZnS/(ZnS+ZnO) ratios calculated based on the intensity change of the S $2p_{1/2}$ XPS signal, confirming this approach. The averaged ZnS/(ZnS+ZnO) compositions for the buffer layers deposited on CIS substrates are 0.99±0.02, 0.94±0.06, 0.80±0.05, and 0.78±0.05 for the 3, 6, 9, and 13.5 min samples, as shown as bullets in Fig. 4. The given error represents the standard deviation of each independently determined ZnS/(ZnS+ZnO) value from the corresponding mean composition.

At the top of Fig. 4 the layer thickness of the deposited buffer layers is shown as calculated from the attenuation of the In $3d_{5/2}$ under the assumption that a homogeneous layer of pure ZnS covers the CIS substrate. [Note that for the

buffer/CIS sample prepared the longest time (13.5 min) only a minimum thickness is given, which corresponds to the XPS information depth of the In $3d_{5/2}$ photoelectrons (see above), since no respective photoemission line can be observed in the corresponding spectrum.] The estimated layer thicknesses of the buffer layers deposited within 3, 6, 9, and 13.5 min on CIS substrates are (0.4 ± 0.1), (0.6 ± 0.2), (1.5 ± 0.3), and $\geq(5.4\pm1.1)$ nm, respectively.

In order to investigate the postdeposition heat treatment, which takes place in the production process of corresponding solar cell devices by default in ambient air at 200 °C for 5 min—drastically enhancing the device performance of the final solar cell[14,16]—the entire buffer/CIS sample series was annealed in system and thus in UHV after the completion of the XPS and XAES characterizations. However, no major changes of the above findings, especially in terms of buffer composition and thickness, after recharacterization of the postannealed buffer/CIS sample series could be identified. This is in good agreement with the finding that the deposited buffer layers contain no or only minor amounts of thermally decomposable $Zn(OH)_2$. Whether the heat treatment plays a role in the formation and "fine-tuning" of the buffer/CIS *p*-*n* junction, especially with respect to possible intermixing processes[34] or whether annealing in ambient air instead of in UHV is important in order to saturate possible defects by oxygen has to be clarified in future experiments.

IV. SUMMARY AND CONCLUSION

A set of samples, where an alternative Zn-compound buffer was deposited during different deposition times (3–13.5 min) on CIS/Mo/glass absorber substrates, was characterized by XPS and XAES in order to investigate the growth mechanism of the buffer in terms of its (surface) composition. We have found that in the early stages of the used alternative CBD process (3 and 6 min samples) a thin [up to (0.6 ± 0.2) nm] ZnS layer is formed on the CIS, whereas in the second half of the CBD (9 and 13.5 min samples) Zn(S,O) with a ZnS/(ZnS+ZnO) ratio of ~80% is deposited with a greatly increased growth rate. After a deposition time of 13.5 min this ZnS/Zn(S,O) bilayer buffer covers the rough CIS absorber substrate completely and is thus $\geq(5.4\pm1.1)$ nm thick. No major changes of these findings after a postannealing of the buffer/CIS sample series in UHV and recharacterization could be identified.

By extending this idea of a graded buffer composition, especially towards a more ZnO-like composition at the top, one might be able to even replace the intrinsic part of the window bi-layer as suggested by the window extension layer concept.[35]

However, the impact of our findings of a graded buffer composition with regard to the (theoretical) considerations of the electronic situation at the buffer/CIS interface and especially whether the pictures of the band alignment drawn in the past have to be reevaluated has to be experimentally clarified in the future.

[1]K. Ramanathan *et al.*, Prog. Photovoltaics **11**, 225 (2003).
[2]M. A. Contreras, K. Ramanathan, J. AbuShama, F. Hasoon, D. L. Young, B. Egaas, and R. Noufi, Prog. Photovoltaics **13**, 209 (2005).
[3]J. Klaer, J. Bruns, R. Henninger, K. Siemer, R. Klenk, K. Ellmer, and D. Bräunig, Semicond. Sci. Technol. **13**, 1456 (1998).
[4]K. Siemer, J. Klaer, I. Luck, J. Bruns, R. Klenk, and D. Bräunig, Sol. Energy Mater. Sol. Cells **67**, 159 (2001).
[5]J. Klaer, I. Luck, A. Boden, R. Klenk, I. Perez, and R. Scheer, Thin Solid Films **431–432**, 534 (2003).
[6]T. Nakada and M. Mizutani, Jpn. J. Appl. Phys., Part 2 **41**, L165 (2002).
[7]R. N. Bhattacharya, M. A. Contreras, and G. Teeter, Jpn. J. Appl. Phys., Part 2 **43**, L1475 (2004).
[8]K. Kushiya, M. Ohshita, I. Hara, Y. Tanaka, B. Sang, Y. Nagoya, M. Tachiyuki, and D. Yamase, Sol. Energy Mater. Sol. Cells **75**, 171 (2003).
[9]M. A. Contreras, T. Nakada, M. Hongo, A. O. Pudov, and J. R. Sites, Proceedings of the Third World Conference on Photovoltaic Energy Conversion (WCPEC-3), Vol. 1, Japan (Arisumi Printing Inc., 2003), p. 570.
[10]A. Ennaoui, Can. J. Phys. **77**, 723 (1999).
[11]A. Ennaoui, S. Siebentritt, M. C. Lux-Steiner, W. Riedl, and F. Karg, Sol. Energy Mater. Sol. Cells **67**, 31 (2001).
[12]A. Ennaoui, W. Eisele, M. C. Lux-Steiner, T. P. Niesen, and F. Karg, Thin Solid Films **431–432**, 335 (2003).
[13]S. Neve, W. Bohne, J. Klaer, R. Klenk, and R. Scheer, Proceedings of the 17th European Photovoltaic Solar Energy Conference (Eu-PVSEC-17), Munich, Germany (WIP Munich 2001), p. 1102.
[14]A. Ennaoui, M. Bär, J. Klaer, T. Kropp, R. Sáez-Araoz, and M. C. Lux-Steiner, Prog. Photovoltaics (in press).
[15]A. Ennaoui, T. Kropp, and M. C. Lux-Steiner, German Patent No. 10 2004 040 546.8–33 (pending).
[16]A. Ennaoui, M. Bär, J. Klaer, T. Kropp, R. Sáez-Araoz, and M. C. Lux-Steiner, Proceedings of the 20th European Photovoltaic Solar Energy Conference (Eu-PVSEC-20), Barcelona, Spain (WIP Munich, 2005), p. 1882.
[17]S. D. Sartale, B. R. Sankapal, A. Ennaoui, and M. C. Lux-Steiner, Thin Solid Films **480–481**, 168 (2005).
[18]*Gmelins Handbuch der Anorganischen Chemie—Ergänzungsband Zink, Syst.-Nr. 32*, edited by E. H. E. Pietsch (Verlag Chemie GmbH, Weinheim, 1956).
[19]M. Bär *et al.*, J. Appl. Phys. (submitted).
[20]N. A. Allsop, A. Schönmann, H.-J. Muffler, M. Bär, M. C. Lux-Steiner, and Ch.-H. Fischer, Prog. Photovoltaics **13**, 607 (2005).
[21]N. A. Allsop (private communication).
[22]I. Lauermann *et al.*, Mater. Res. Soc. Symp. Proc. **763**, B4.5.1 (2003).
[23]D. Briggs and M. P. Seah, *Auger and X-ray Photoelectron Spectroscopy*, Practical Surface Analysis Vol. 1 (Wiley, New York, 1990).
[24]S. Tanuma, C. J. Powell, and D. R. Penn, Surf. Interface Anal. **21**, 165 (1993).
[25]S. Tougaard, QUASES-IMFP-TPP2M code for the calculation of the inelastic electron mean free path, Version 2.2, http://www.quases.com/
[26]L. S. Dake, D. R. Baer, and J. M. Zachara, Surf. Interface Anal. **14**, 71 (1989).
[27]NIST X-Ray Photoelectron Spectroscopy Database, NIST Standard Reference Database 20, Version 3.4, http://srdata.nist.gov/xps/
[28]C. D. Wagner, W. M. Riggs, L. E. Davis, and J. F. Moulder, in *Handbook of X-ray Photoelectron Spectroscopy*, edited by G. E. Muilenberg (Perkin-Elmer Corporation, Eden Prairie, 1979).

[29]I. Lauermann *et al.* (unpublished).

[30]L. Weinhardt *et al.*, Appl. Phys. Lett. **82**, 571 (2003).

[31]R. Hunger, T. Schulmeyer, A. Klein, W. Jaegermann, M. V. Lebedev, K. Sakurai, and S. Niki, Thin Solid Films **480–481**, 218 (2005).

[32]M. Bär *et al.*, Appl. Phys. Lett. **86**, 222107 (2005).

[33]K. Ramanathan *et al.*, Proceedings of the 26th IEEE PVSC, Anaheim, USA (IEEE, conference paper), 1997, p. 319.

[34]M. Bär *et al.*, J. Appl. Phys. (unpublished).

[35]M. Bär, Ch.-H. Fischer, H.-J. Muffler, S. Zweigart, F. Karg, and M. C. Lux-Steiner, Sol. Energy Mater. Sol. Cells **75**, 101 (2003).